JOURNAL OF AIRCRAFT
Vol. 34, No. 4, July–August 1997

Blade–Vortex Interaction Noise Prediction Using a Rotor Wake Roll-Up Model

G. Rahier* and Y. Delrieux*
ONERA, Châtillon 92322, France

The theoretical methods used at ONERA for the blade–vortex interaction (BVI) noise prediction are described. Predictions are performed in five main steps: rotor trim, wake geometry, interacting vortices, blade pressure, and radiated noise. Three ways of introducing the wake influence in unsteady load computations are investigated. The first one assumes that the tip filaments of the wake lattices are dominant. The second one treats all of the filaments of the lattices as interacting vortices. The last one aims at modeling the local wake rolling-up and the vortex concentration. For each method, theoretical vortex geometries and intensities, loads, contours plots, and acoustic signatures are presented and compared to experiment. They show the benefit of using a roll-up model for BVI noise predictions. Indeed, the tip filament assumption appears to not be general enough for realistic applications and the whole lattice approach does not seem reliable. On the contrary, fairly good aeroacoustic results are achieved using the roll-up model. Particularly, this modeling allows us to deal with rotor geometries and kinematics that are likely to generate inboard vortices.

Nomenclature

C = chord length
C_n = lift coefficient
C_T = thrust coefficient
M = Mach number of a blade section
R = rotor radius
r = spanwise location
T = rotor rotation period
α_{shaft} = shaft angle of the rotor
α_{TPP} = tip path plane angle of the rotor
Γ = circulation on a blade section
$\tilde{\Gamma}$ = nondimensional circulation, $\Gamma/\Omega RC$
ψ = azimuth of the reference blade, 0 deg downstream
Ω = rotor rotational speed

Introduction

BLADE–vortex interaction (BVI) noise is a major component of the noise radiated by helicopters in descent flight. Because of the nuisance for people living near heliports, noise is presently a key issue for the development of the civil market of helicopters. Consequently, BVI noise prediction has received much attention over the years.

BVI noise is caused by impulsive load fluctuations occurring on the blades when they interact with intense, concentrated vortices generated by preceding blades. The prediction of blade load using computational fluid dynamics-type flow solvers without any integral wake model[1,2] is not yet accurate enough for BVI noise applications. This is mainly because of the difficulty of capturing and following small concentrated vortex structures in the midst of an extended three-dimensional time-dependent flow. For this reason, most current BVI aeroacoustic approaches use integral wake models to simulate the vortex disturbances in load computations. Typically, the rotor wake is described as one vortex lattice (vortex mesh) per blade with an empirical geometry (prescribed wake)[3] or with a geometry calculated using the local velocity field (free wake).[4,5]

Presented as Paper 95-053 at the CEAS/AIAA 1st Joint Aeroacoustics Conference, Munich, Germany, June 12–15, 1995; received June 15, 1995; revision received March 7, 1997; accepted for publication March 9, 1997.

*Engineer, Acoustic Department.

In this paper the velocity field induced by each vortex lattice is introduced in the load computations using three different techniques.

Tip Filaments Wake Approach

This model assumes that the actual vortex sheet rolls-up in a single vortex emitted at the blade tip. Moreover, it is assumed that the actual inboard sheet does not produce impulsive load fluctuations. The actual tip vortex is modeled by the outboard tip filament of the numerical vortex lattice. Its location and induced velocity field are computed at each time step of the load calculation. An adapted spanwise mesh (not too refined at the blade tip) is needed so that the circulation of the actual vortex is not shared among several filaments of the lattice, but is concentrated on the tip filament. The inboard sheet influence on loads is introduced by the velocity field induced by the inboard lattice. The high frequencies of this velocity field are filtered to avoid fluctuations caused by the inboard sheet discretization.

Whole Lattice Wake Approach

In this approach, no physical assumption is made about the wake roll-up. It is theorized that the computation of the lattice convection is able to correctly predict the local wake rolling-up and the vorticity concentration. The sheet influence on loads is introduced by the velocity field induced by all of the filaments of the vortex lattice. No distinction is made between the filaments that are thus considered to be potential interacting vortices.

Roll-Up Wake Approach

In this method, as in the preceding approach, no assumption is made about the number and location of the actual interacting vortices, but the local rolling-up and the vorticity concentration are modeled. One or several new vortex filaments are constructed, based on the characteristics of the vortex lattices. These filaments simulate the actual vortices in circulation and location. They do not generally coincide with filaments of the vortex lattice. Portions of the vortex lattice not accounted for by the constructed vortices are treated as an inboard sheet in the load computations (see the Tip Filaments Wake Approach section).

In this paper, the outcomes of the wake model approaches on the predicted blade loads and on the radiated noise are analyzed for two descent flight cases of the recent higher harmonic control aeroacoustic rotor tests (HART) (Ref. 6). These two cases are particularly well suited for this study because they provide very different types of trailed vorticity. The theoretical tools used, the experimental setup, and the selected test cases are briefly described. The aerodynamic and acoustic results are analyzed. The benefit of a wake roll-up model in BVI noise prediction is emphasized.

Aeroacoustic Prediction Methods

BVI noise is predicted at ONERA using a five-stage process: 1) the rotor is trimmed to the actual flight or test conditions, 2) the rotor wake is computed, 3) the interacting vortices are then determined in geometry and circulation, 4) the local blade surface pressures are calculated as a function of azimuth, and 5) the sound radiation is predicted using this blade surface pressure distribution as input.

Rotor Trim

An aeroelastic code [R85/METAR (Ref. 7): aerodynamic comprehensive rotor model], initially developed by Eurocopter France, is used to trim the rotor by taking into account aerodynamic, inertial, and elastic forces and moments on the blades.

The R85 code computes the dynamic (quasisteady) response and elastic deformations in torsion, flap, and lag by solving the Lagrange equations in which the elastic energy is written using a linear beam model. The aerodynamic model is based on a lifting-line method. The aerodynamic coefficients C_l, C_m, and C_d are directly read in two-dimensional airfoil tables taking into account compressibility and viscous effects. Then, they are corrected for Reynolds number, and linear unsteady effects (Theodorsen theory) are added for the C_m coefficient.

In the METAR code, the rotor wake is described by vortex lattices, the geometry of which is prescribed depending on the rotor trim. A coupling between R85 and METAR is made until convergence on induced velocities on the rotor disk is achieved, so that the rotor trim accounts for vortical wake and blade elasticity, which can be very important as proven in Ref. 8.

Wake Geometry

The prescribed wake geometry deduced from R85/METAR is distorted using a free-wake analyzing (MESIR) code,[5] assuming that distorting the wake does not significantly change the rotor trim. Note that the geometry of the entire wake is distorted in the wake deformation process and not just the tip filaments. Geometric modifications of the wake are continued until convergence on the spanwise distribution of the local blade-bound circulation (three iterations are enough in practice). The wake emitted during three rotor revolutions is described by 10 filaments in the spanwise direction with an azimuthal step of 10 deg.

The predicted wake is input directly into the calculation of the blade pressure fluctuations when using the tip filaments wake approach or the whole lattice approach. The roll-up model described next is introduced between wake and pressure calculations when using the roll-up vortex wake approach.

Wake Roll-Up

The wake roll-up is modelized starting from the results of the free-wake analysis (circulation Γ and location x, y, z of the wake filaments). The circulation Γ_v and location x_v, y_v, z_v of the rolled-up vortices are predicted using the following procedure (code MENTHE: roll-up modeling of the vortex sheet of a helicopter rotor).

The vortical intensity $\partial\Gamma(r)/\partial r$ of the local trailed wake is approximated at each blade azimuth by $(\Gamma_{i+1} - \Gamma_i)/(r_{i+1} - r_i)$,

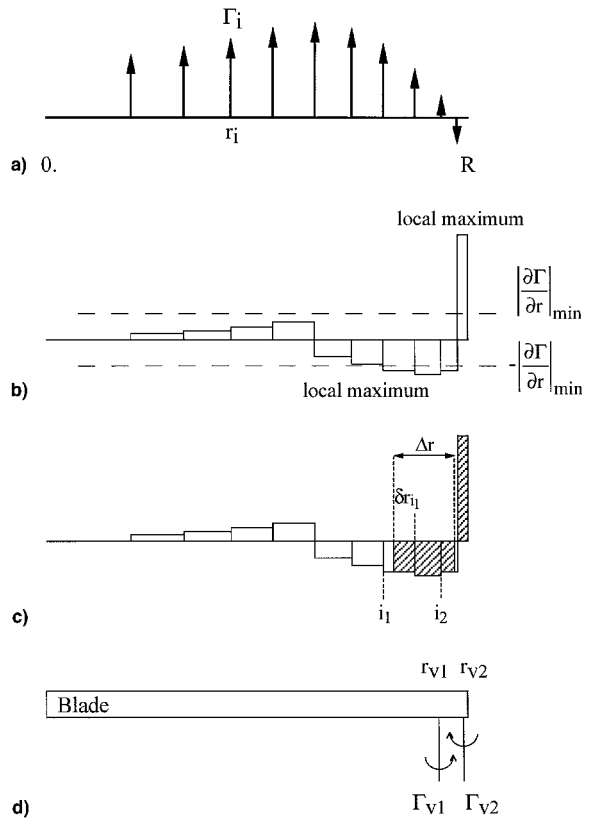

Fig. 1 Procedure of the roll-up wake model: a) discretized blade bound circulation, b) vortical intensity, c) intensity summing up, and d) constructed vortices.

where Γ_i is the blade bound circulation at the radial position r_i (Figs. 1a and 1b).

The local maxima in $\partial\Gamma(r)/\partial r$ (above a threshold inspired of rotor wind-tunnel tests[9]) are identified (Fig. 1b). This threshold expresses the requirement of a shear in the vortical wake strong enough to result in a roll-up before the interaction with a following blade occurs.

The circulation Γ_v of each rolled-up vortex is obtained by summing up the vortical intensity over a spanwise portion Δr, depending on the level of the corresponding local maximum (Fig. 1c):

$$\Gamma_v = \sum_{i=i_1}^{i_2} \delta r_i \frac{(\Gamma_{i+1} - \Gamma_i)}{(r_{i+1} - r_i)} \quad \text{and} \quad \Delta r = \sum_{i=i_1}^{i_2} \delta r_i$$

The radial location r_v at the emission time of the constructed vortex is calculated using the following formula (Fig. 1d):

$$r_v = \left(\sum_{i=i_1}^{i_2} k_i r_i\right) \Big/ \left(\sum_{i=i_1}^{i_2} k_i\right)$$

where $k_i = r_i \delta r_i (\Gamma_{i+1} - \Gamma_i)/(r_{i+1} - r_i)$.

The coefficients k_i used in this barycenter rule have been chosen to give a larger weight to the outboard part of the vortex lattice.

The vortices constructed in such a way at each blade azimuth are joined together in agreement with the continuity of an actual roll-up.

The trajectory $x_v(t)$, $y_v(t)$, $z_v(t)$ of the constructed vortices is computed starting from the trajectory $x_i(t)$, $y_i(t)$, $z_i(t)$ of the wake filaments provided by the free-wake analysis. This tra-

jectory is obtained using the barycenter rule previously defined for the computation of r_v at the emission time:

$$x_v(t) = \left[\sum_{i=i_1}^{i_2} k_i x_i(t)\right] \Big/ \left(\sum_{i=i_1}^{i_2} k_i\right)$$

and similar formulas for $y_v(t)$ and $z_v(t)$.

This set of routines results in interacting vortices, the location and the circulation of which are nearly independent of the mesh used in the free-wake analysis. (Actual vortices are also generated at the blade root as a result of the local circulation jump. These vortices do not contribute to BVI noise. In practice, they are not constructed by the roll-up procedure.)

Blade Pressure

Blade pressure distribution is computed using a two-dimensional singularity method (ARHIS code: aerodynamic of helicopter rotor–wake interactions).[10] ARHIS predicts unsteady flows in incompressible and inviscid fluids. The three-dimensional problem is solved using a repetitive two-dimensional strip analysis. The flow relative to each blade section is deduced from an analysis of the interacting vortices and is defined to simulate as close as possible to the real three-dimensional phenomenon. Finite span effects are introduced through an elliptic-type correction on the pressure coefficients. The subsonic compressibility effects are included by means of Prandtl–Glauert corrections associated with local thickening of the airfoil. In the case of strong interaction, the vortex is modeled as a cloud of elementary vortices to take its deformation into account. The vortex viscous core radius is calculated starting from the vortex circulation and its age at the interaction time, which are parameters provided by the wake analysis using an empirical correlation derived from experimental results.[10] This correlation has been recently improved using the laser Doppler velocimetry (LDV) measurements acquired during the HART test program Ref. 11. The viscous core radius of the noisiest vortices is about 25% chord in the present calculations.

Noise Radiation

The noise radiation is computed by the acoustic prediction of rotor–wake interaction (PARIS) code,[12] starting from the pressure distribution provided by ARHIS. PARIS is based on the Ffowcs Williams and Hawkings equation and predicts the loading and thickness noise. It uses a time-domain formulation. An efficient spanwise interpolation method has been implemented in the code to minimize the amount of airload data required for BVI noise prediction. This interpolation allows the aerodynamic and acoustic CPU time to be reduced by a factor of 3.

Experimental Setup and Selected Cases

The experimental results from the HART test program[6] (which was performed in the Duits–Nederlandse Windtunnel (DNW) 6 × 8 m open test section) are compared with predictions in this paper. These tests were jointly conducted by the U.S. Army/DLR/DNW/NASA and ONERA. Their objective was to gain a physical understanding of the mechanisms involved in BVI from both experimental and theoretical points of view. They provided a unique database for validating aerodynamic and acoustic codes. More detailed information can also be found in Ref. 11. Note that the present paper does not deal with higher harmonic control (HHC) effects on noise and vibration.

Model Rotor

The model rotor is a 40% dynamically scaled model of a hingeless BO105 main rotor. Its main characteristics are the following: four blades, 2 m radius, 0.121 m chord length, rectangular planform, −8 deg (root to tip) linear twist, 2.5-deg precone angle, modified NACA 23012 airfoil, and 1050 rpm rotor nominal operating speed.

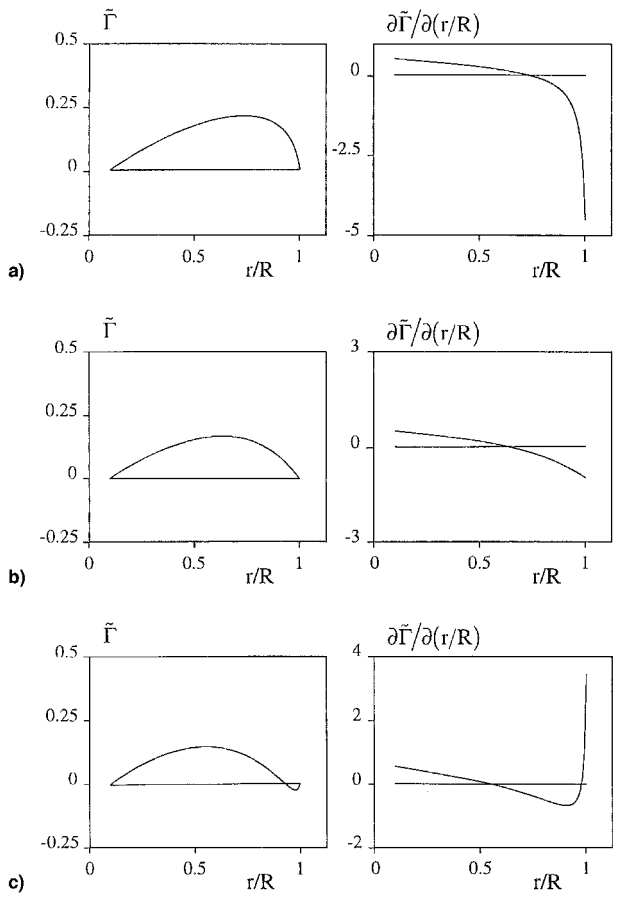

Fig. 2 Main types of blade-bound circulation and trailed vorticity: a) type 1, strong loads; b) type 2, medium loads; and c) type 3, negative tip load.

Instrumentation

The blades were instrumented with 124 pressure transducers distributed mainly at three spanwise stations located at r/R = 0.75, 0.87, and 0.97. Integration of chordwise pressure measurements provides the time history of the local C_nM^2 lift coefficient for each section. Acoustic measurements were recorded by 11 microphones mounted on a traversing rake system located 2.4 m underneath the rotor. The sound pressure time histories of each microphone were acquired for a set of streamwise positions of the traversing rake system. Flowfield visualizations were performed by using a laser light sheet (LLS) system. Certain test cases were studied in greater detail and the positions of the interacting vortices were identified on both advancing and retreating sides. Blade deflection measurements were also performed by using several techniques explained in Ref. 11. They provided the blade deformations (bending and torsion) and the blade tip attitude at given azimuths.

Selected Test Cases

The present study uses data from two runs of the HART tests. Both simulate a 6-deg descent flight path for an advance ratio μ = 0.15, C_T = 0.0044, α_{shaft} = 5.3 deg, and α_{TPP} = 3.8 deg. The first case (run 140) has a monocyclic control law. The second case (run 133) has a 3/revolution HHC law. These two runs are particularly well suited for the analysis of the trailed vorticity. Indeed, the control law combined with the blade elasticity leads to various spanwise distributions of blade circulation, and consequently, to various trailed vorticity distributions.

Types of Blade-Bound Circulation and Trailed-Wake Vorticity

For conventional blade geometries (no flap, no vane-tip), there are mainly three types of spanwise distribution of blade-bound circulation (Fig. 2). Type 1 can be connected with strong loads, generally occurring on the retreating blade. The wake vortical intensity that is related to $d\Gamma/dr$ on the blade is then concentrated at the blade tip (Fig. 2a). Type 2 corresponds to lower loads, more typical of the advancing blade. In this case, the vortical intensity is more evenly distributed (Fig. 2b). Finally, type 3 occurs, for example, when a strong negative torsion added to the static twist results in negative angles of attack at the blade tip. Two maxima of opposite sign are then found in the trailed vorticity (Fig. 2c), and two vortices of opposite sense of rotation can be generated: 1) an inboard vortex linked to the positive blade load (the main load) and 2) a tip vortex created by the negative tip load.

From the numerical point of view, these types of blade-bound circulations lead to the following distributions of circulation in the vortex lattice. For type 1 loading, the circulation of the tip filament is clearly dominant. Conversely, in type 2 loading, the trailed vorticity is distributed on several outboard filaments, the number of which depends on the wake discretization near the blade tip. For type 3, the trailed vorticity linked to the main blade load is distributed on inboard filaments, and the vorticity caused by the tip load is trailed by the tip filament.

These three main kinds of blade-bound circulation distribution and trailed-wake vorticity are encountered in runs 140 and 133. They will be used later to discuss the aeroacoustic results according to the way the wake influence is introduced in the load calculations.

Theoretical Predictions and Comparisons with Experiment

Interacting Vortex Geometries and Circulations

The top views of the vortex lattice relative to one blade predicted by the free-wake analysis (MESIR code) are plotted in Figs. 3a and 3b for both runs. They represent frozen wake patterns for the blade at ψ = 180-deg azimuth. On the figures, the tip filament is drawn as the straight line. The vortices obtained using the roll-up model are plotted on the Figs. 3c and 3d. For run 140, the blade-bound circulation is type 1 on the retreating side and type 2 on the advancing side. Thus, the roll-up model predicts only one vortex, located at or near the blade tip [outboard vortex (OV)]. For run 133, the blade-bound circulation on the advancing side is type 3 at certain azimuths. The roll-up model constructs two vortices at these azimuths, one at the blade tip (OV), another one more inboard [inboard vortex (IV)]. At the other azimuths, the blade-bound circulation is type 1 or 2 as for run 140 and only one vortex is constructed by the roll-up model. The main vortex (in terms of circulation) is represented as the straight line. It is not always found at the blade tip. At the azimuths where it slides inboard, the secondary vortex (dashed line), located at the blade tip, has a contrary sense of rotation.

The results provided by the roll-up wake approach are very consistent with the flow visualizations done during the HART test program. On the advancing side, these visualizations have shown a single vortex (per blade) for run 140 and the presence of two vortices of opposite sense of rotation for run 133, as reported in Ref. 11.

The blade–vortex vertical miss-distance at the interaction time is of great interest because it is a determinant parameter of the radiated sound. The predicted miss-distances relative to the interactions of a blade with its own vortex lattice on the advancing side (the noisiest side) are plotted in Fig. 4, with the same display as in Fig. 3. This figure shows that, for both runs, the whole lattice approach introduces numerous inboard filaments in close interaction with the blade.

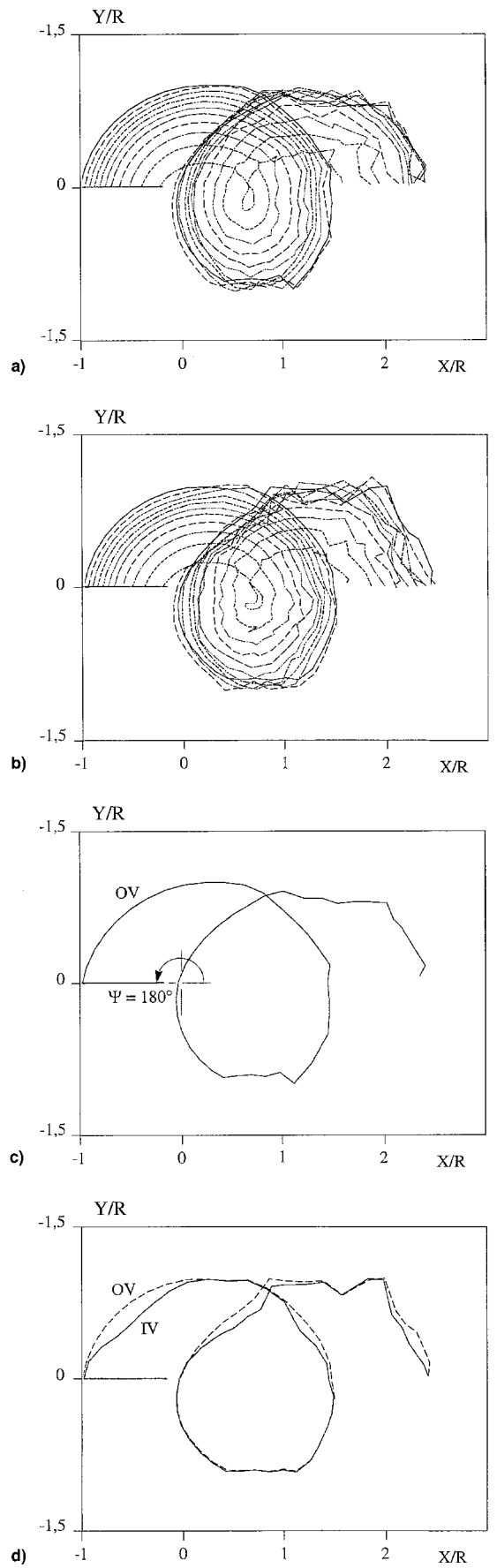

Fig. 3 Top view of the vortex lattice and of the constructed vortices (relative to one blade): a) run 140, MESIR vortex lattice; b) run 133, MESIR vortex lattice; c) run 140, MENTHE constructed vortex; and d) run 133, MENTHE constructed vortices.

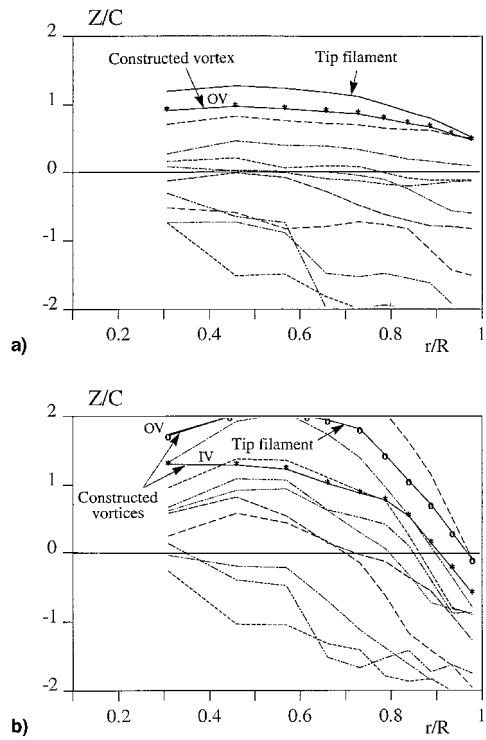

Fig. 4 Predicted blade–vortex vertical miss-distances on the advancing side, at the interaction time. Vortex lattice and constructed vortices relative to one blade: a) run 140 and b) run 133.

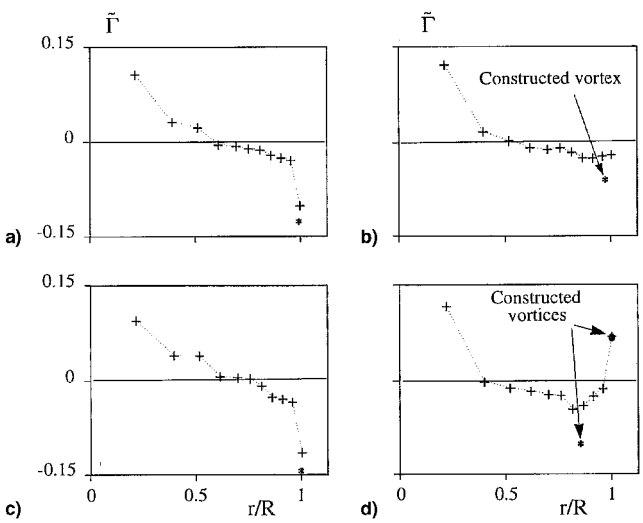

Fig. 5 Predicted vortex circulations of the wake lattice and of the constructed vortices, at the emission azimuths of the interacting vortices: a) run 140, ψ = 225 deg; b) run 140, ψ = 135 deg; c) run 133, ψ = 225 deg; and d) run 133, ψ = 135 deg.

For run 140, the miss-distances deduced from the tip filament assumption or from the roll-up model differ slightly (Fig. 4a). Indeed, as the trailed vorticity on the advancing side is type 2, inboard wake filaments and not only the tip filament take part in the computation of the trajectory of the single vortex predicted by the roll-up model.

For run 133, the trailed vorticity is type 3 at the azimuths where the interacting vortices on the advancing side are generated. Because of the concentration of the positive trailed vorticity at the blade tip (Fig. 2c), the outboard rolled-up vortex coincides with the tip filament (Fig. 4b). The inboard vortex predicted by the roll-up model interacts with the blade with the small vertical miss-distances. This inboard vortex has a preponderant contribution to the radiated noise, as will be shown in the Acoustic Results section.

The discussion concerning the vortex lattice emitted by the other blades would lead to the same comments.

The circulation of the filaments of the wake lattice (including the tip filament) and the circulation of the rolled-up vortices are presented in Fig. 5 for the emission azimuths of the interacting vortices: ψ = 225 deg on the retreating side and ψ = 135 deg on the advancing side.

For run 140, the trailed vorticity is type 1 on the retreating side (Fig. 5a). Thus, the rolled-up vortex is only slightly stronger in circulation (about +30%) than the tip filament and the circulation of the inboard filaments are much lower. Conversely, on the advancing side (Fig. 5b), the circulation of the tip filament is of the same order as the circulation of neighboring inboard filaments (type 2 trailed vorticity). At these azimuths, the circulation of the rolled-up vortex, resulting in the summing up of the vortical intensity over a spanwise portion, is about three times stronger than the circulation of the tip filament.

For run 133, the previous comments about the circulations on the retreating side are still valid (Fig. 5c, type 1 trailed vorticity). On the advancing side (Fig. 5d), the main vortex (inboard) predicted by the roll-up model, has a rather higher circulation (negative) than any inboard filament. The secondary rolled-up vortex, present only in this azimuthal area, has the circulation of the tip filament (type 3 trailed vorticity).

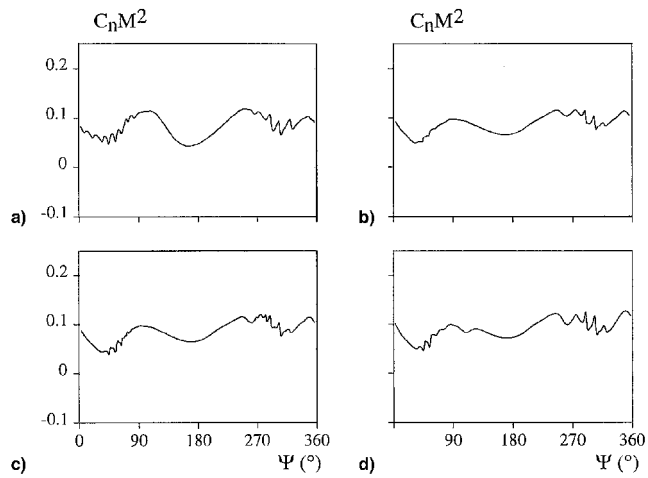

Fig. 6 Measured and predicted section loads for run 140 (r/R = 0.87): a) experiment, b) tip filament approach, c) whole lattice approach, and d) roll-up wake approach.

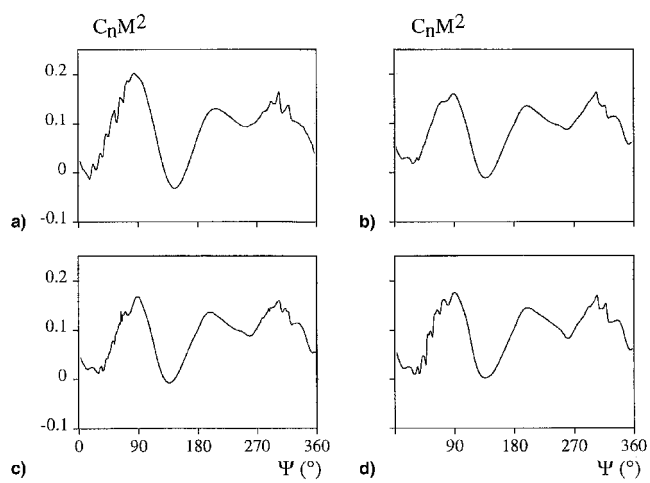

Fig. 7 Measured and predicted section loads for run 133 (r/R = 0.87): a) experiment, b) tip filament approach, c) whole lattice approach, and d) roll-up wake approach.

The interacting vortex circulation is an important parameter in the BVI noise generation. The discrepancies in circulation partly explain the differences between noise predictions performed using the tip filament assumption, the whole lattice approach, or the roll up vortex method, as will be shown in the sections devoted to the aerodynamic and acoustic results.

Local Blade Loads

For both runs, the low-frequency components of the C_nM^2 coefficient at $r/R = 0.87$ are in good agreement with experiment, regardless of the method used (discussed in the Introduction) (Figs. 6 and 7). It only means that the low-frequency components of the wake influence on the loads are correctly predicted by the three theoretical methods, but these components are not related to the BVI noise. However, the high-frequency components of the predicted loads exhibit more or less BVI peaks, depending on the method. This is particularly obvious on the advancing side for run 133. Unfortunately, the C_nM^2 plots do not provide direct precise information of the BVI acoustic source intensities as the load time-derivatives do (as shown in Ref. 10).

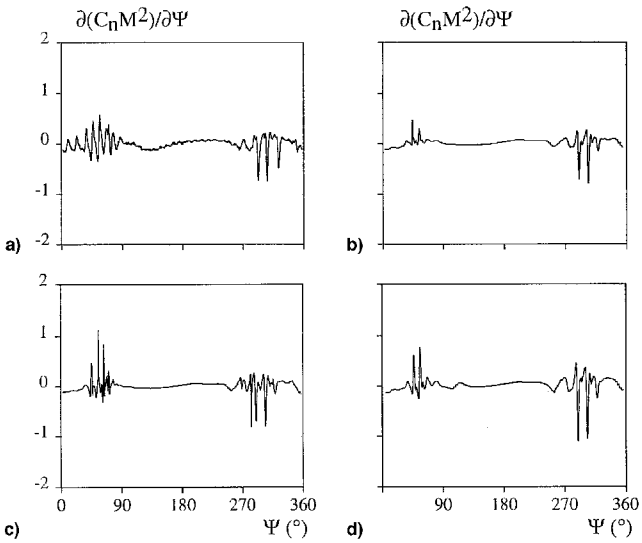

Fig. 8 Measured and predicted section load time-derivatives for run 140 ($r/R = 0.87$): a) experiment, b) tip filament approach, c) whole lattice approach, and d) roll-up wake approach.

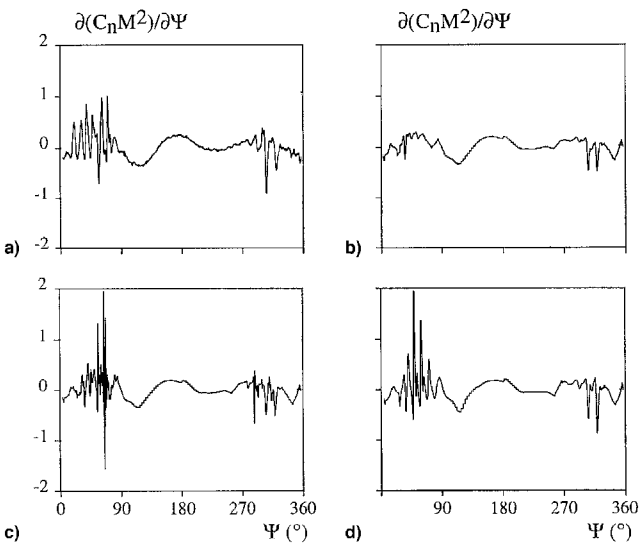

Fig. 9 Measured and predicted section load time-derivatives for run 133 ($r/R = 0.87$): a) experiment, b) tip filament approach, c) whole lattice approach, and d) roll-up wake approach.

These section load time-derivatives are displayed in Figs. 8 and 9. The consequences of the method used to introduce the wake influence in load computations clearly appear. On the retreating side ($\psi > 180$ deg), the acoustic sources calculated either using the tip filament assumption or the roll-up model are comparable to the measurements for both runs. Particularly, the phases of the BVI peaks are well predicted. It means that the actual interacting vortices are probably emitted near the blade tip. The computed relative amplitudes can easily be related to the vortex circulations previously investigated. The whole lattice approach leads to rather different results with more peaks than in the experiment.

Differences are even more obvious on the advancing side ($\psi < 180$ deg), where the number and amplitude of the BVI peaks vary very much from one analysis to another. Using the tip filament assumption, the BVI peaks are dramatically underestimated, both in number and amplitude, because the inboard vortices are not taken into account and the circulation of the outboard vortices is underestimated. Using the whole lattice approach, many peaks appear that are not correlated with experiment, particularly in run 133 (Fig. 9c). Indeed, contrary to a concentrated roll-up, several separate filaments provide separate unrealistic BVI peaks, the number of which obviously depends on the wake discretization. The roll-up model leads to acoustic sources more similar to the experiment, even if the number (run 140) or amplitude (run 133) of the BVI peaks do not completely match the experiment.

Acoustic Results

Noise Contours

To estimate the BVI impulsive noise content, the experimental as well as theoretical noise contour plots have been derived, respectively, from measured and calculated acoustic signals, at the nodes of a grid situated 2.4 m underneath the rotor (Fig. 10). The measurements and the predicted sound pressures have been filtered in a bandwidth corresponding to the 6th to 40th blade passage harmonic (representative of BVI noise). The experimental time signatures used for the frequency analysis were sampled and averaged in synchronization with the rotation of the rotor shaft to characterize discrete frequency tones (the only sound component addressed here).

The predicted noise contours do not qualitatively (with respect to the shape) differ from one another, depending on the technique used to determine the interacting vortices (Figs. 11 and 12). These time-averaged noise contours are in good agreement with experiment. The locations of local maxima because of the blade–vortex interactions on the retreating and advancing sides are generally correctly identified. Discrepancies are mainly quantitative with respect to the local maximum

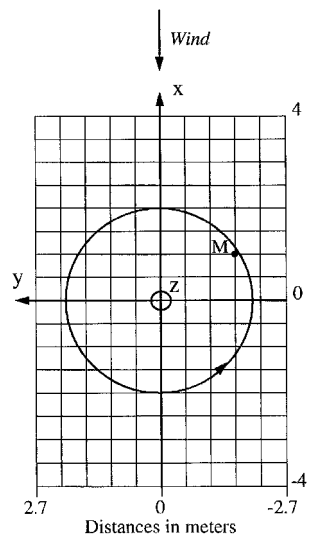

Fig. 10 Top view of the acoustic measurement (and prediction) grid.

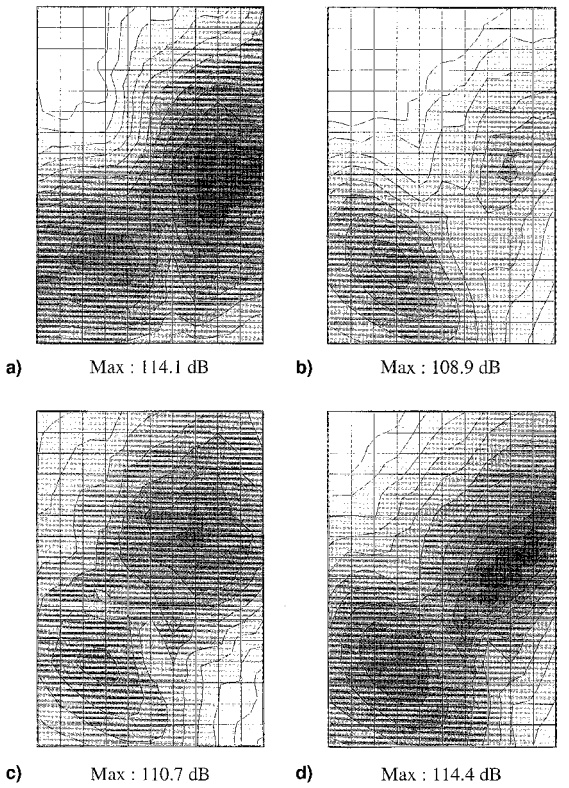

Fig. 11 Measured and predicted noise contours for run 140 (2-dB noise level increment): a) experiment, b) tip filament approach, c) whole lattice approach, and d) roll-up wake approach.

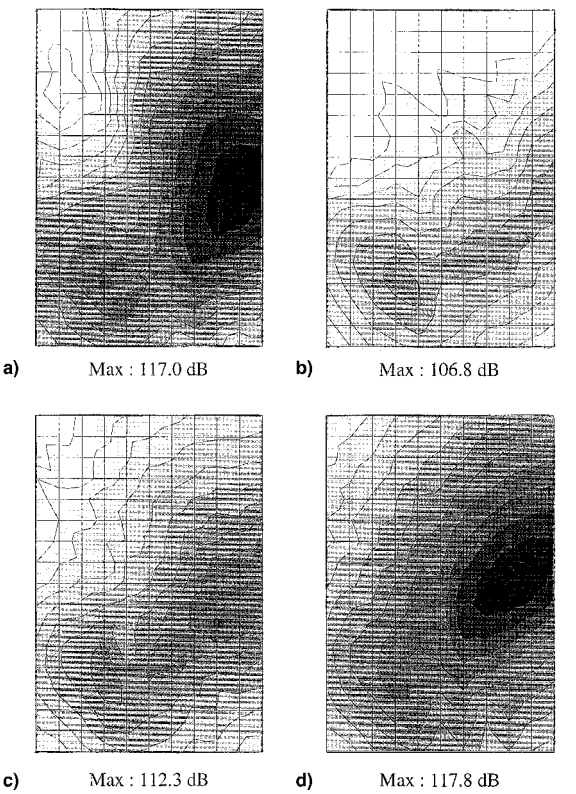

Fig. 12 Measured and predicted noise contours for run 133 (2-dB noise level increment): a) experiment, b) tip filament approach, c) whole lattice approach, and d) roll-up wake approach.

levels. These sound pressure levels confirm the previous analysis of the blade loads: rather comparable values on the retreating side and strong discrepancies on the advancing side where the underpredictions can exceed 10 dB. The maximum levels predicted using the roll-up model differ from measurements by less than 1 dB. These quite good results cannot be achieved with the two other methods. The whole lattice approach seems to bring an improvement as compared to the tip filament assumption. However, this improvement is not reliable since the increases in noise levels are a result of nonphysical peaks.

Acoustic Signature

A more precise investigation of the sound radiation can be done by examining sound pressure time histories. The microphones selected for this are located at each local maximum of the experimental contour plots (X, Y, and Z axis defined in Fig. 10).

Retreating side:

$$\text{run 140: } X = -2 \text{ m; } Y = 1.08 \text{ m, } Z = -2.4 \text{ m}$$

$$\text{run 133: } X = -2.5 \text{ m; } Y = 1.08 \text{ m, } Z = -2.4 \text{ m}$$

Advancing side:

$$\text{run 140: } X = 0; \; Y = -2.16 \text{ m, } Z = -2.4 \text{ m}$$

$$\text{run 133: } X = -0.5 \text{ m; } Y = -2.16 \text{ m, } Z = -2.4 \text{ m}$$

On the retreating side (Figs. 13 and 14), the experimental signatures are characterized by a dominant impulsive peak, which is reproduced fairly well by all of the computations. This is not surprising because, for the two runs, the spanwise distribution of blade-bound circulation on the retreating side is type 1. The wake vortical intensity is concentrated at the blade tip, and consequently, the influences of the whole lattice, the tip filament, and the constructed vortex are quite close.

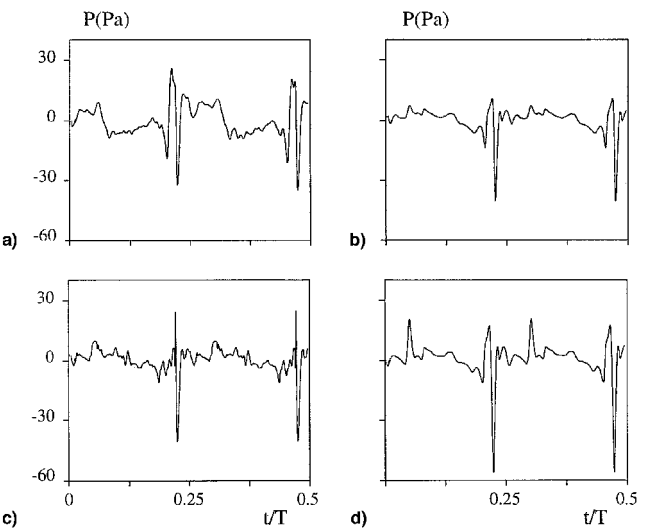

Fig. 13 Measured and predicted acoustic signatures for run 140 (retreating side): a) experiment, b) tip filament approach, c) whole lattice approach, and d) roll-up wake approach.

On the advancing side (Figs. 15 and 16), the acoustic signatures are consistent with all of the preceding results. Using the tip filament assumption, which results in underestimating the vortex circulations and excluding the inboard vortices, causes an underestimation of BVI peaks (run 140, Fig. 15b) or a complete lack of BVI peaks (run 133, Fig. 16b). The whole lattice approach seems to better take into account the inboard trailed vorticity that actually has a preponderant contribution to the radiated noise in run 133 (Fig. 16c). However, it leads to peaks that are not in correlation with the measurements (Figs. 15c and 16c). The best results are achieved with the roll-up model (Figs. 15d and 16d).

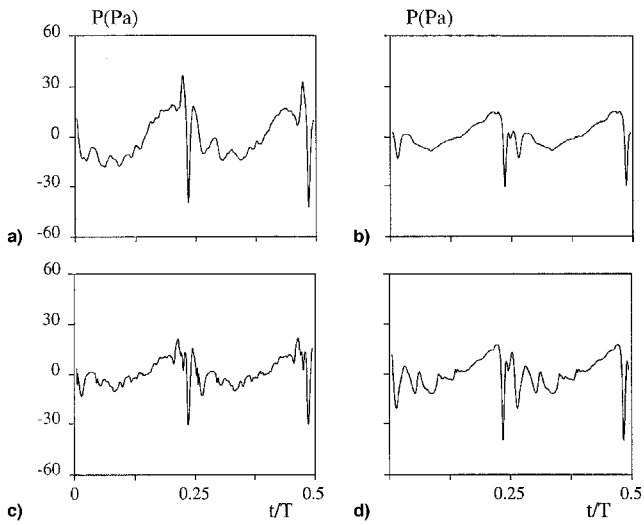

Fig. 14 Measured and predicted acoustic signatures for run 133 (retreating side): a) experiment, b) tip filament approach, c) whole lattice approach, and d) roll-up wake approach.

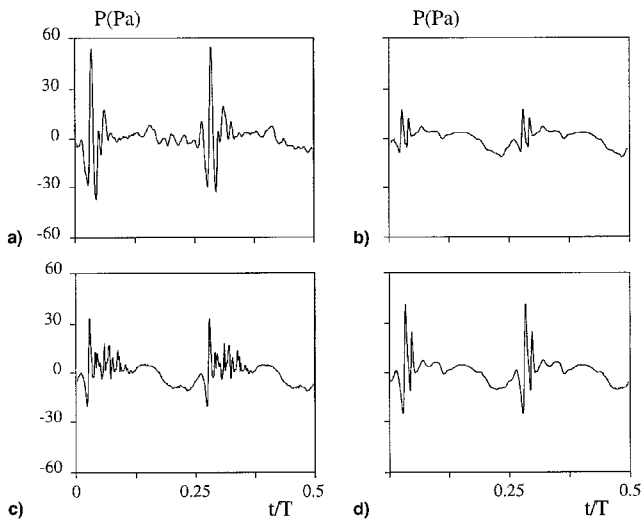

Fig. 15 Measured and predicted acoustic signatures for run 140 (advancing side): a) experiment, b) tip filament approach, c) whole lattice approach, and d) roll-up wake approach.

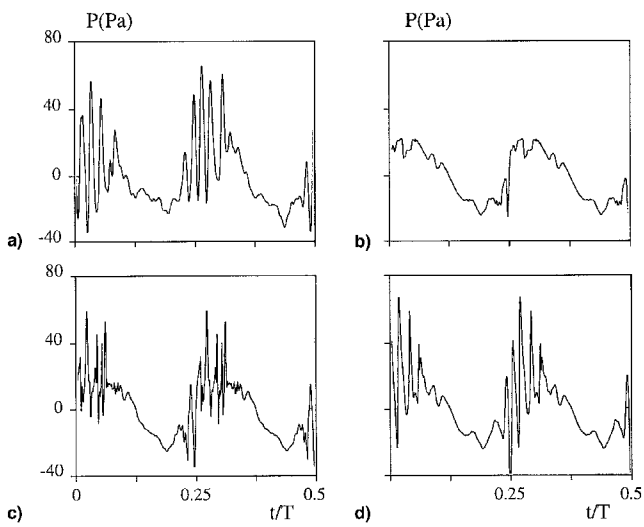

Fig. 16 Measured and predicted acoustic signatures for run 133 (advancing side): a) experiment, b) tip filament approach, c) whole lattice approach, and d) roll-up wake approach.

Conclusions

Three ways of introducing the wake influence in load calculations have been investigated in the frame of BVI noise predictions using integral wake models. The aerodynamic and acoustic results show that the single tip filament model is not general enough for realistic applications to aeroelastic rotors with high aspect ratio. Particularly, this method cannot deal with inboard vortices that may be generated by such rotors. Furthermore, this model leads to vortex circulations that are dependent on the mesh used for the wake calculation.

The whole lattice approach takes into account inboard trailed vorticity, but the local wake rolling-up and the vortical concentration are not well simulated. This method leads to many BVI peaks in the load time evolutions as well as in the acoustic signatures without correlation with measured data. Thus, the method does not seem to be reliable, even if it provides better sound pressure levels than the single-tip filament method.

The roll-up model presently used, which models the local wake rolling-up and the vortical concentration into interacting vortices, leads to much better qualitative and quantitative aerodynamic and acoustic predictions. Indeed, a roll-up wake approach enables one to better predict the tip vortex circulation and to take into account inboard vortices with a realistic number of interacting vortices nearly independent of the mesh used in the free-wake analysis. It must be noted that whatever the complexity of the developed roll-up model may be, the quality of the final result will strongly depend on the accuracy of the calculated wake used as input data. These input data may probably be improved by implementing the roll-up model in the wake computation.

Acknowledgments

The authors are very grateful to all the members of the HART test and prediction teams from U.S. Army, DLR, DNW, NASA, and ONERA, and particularly to the data providers, Alain Boutier, Roland Kube, Wolfgang Wagner, Edzard Mercker, Ulrich Seelhorst, and Wolf Splettstoesser.

References

[1]Srinivasan, G. R., and Baeder, J. D., "Recent Advances in Euler and Navier-Stokes Methods for Calculating Helicopter Rotor Aerodynamics and Acoustics," 4th International Symposium on Computational Fluid Dynamics, Davis, CA, Sept. 1991.

[2]Boniface, J. C., Mialon, B., and Sides, J., "Numerical Simulation of Unsteady Euler Flow Around Multibladed Rotor in Forward Flight Using a Moving Grid Approach," 50th Annual Forum of the American Helicopter Society, Fort Worth, TX, May 1995.

[3]Van der Wall, B., "An Analytical Model of Unsteady Profile Aerodynamics and Its Application to a Rotor Simulation Program," 15th European Rotorcraft Forum, Amsterdam, The Netherlands, Sept. 1989.

[4]Johnson, W., "CAMRAD/JA A Comprehensive Analytical Model of Rotorcraft Aerodynamics and Dynamics," Johnson Aeronautics, Palo Alto, CA, 1988.

[5]Michèa, B., Desopper, A., and Costes, M., "Aerodynamic Rotor Loads Prediction Method with Free Wake for Low Speed Descent Flight," 18th European Rotorcraft Forum, Avignon, France, Sept. 1992.

[6]Yu, Y. H., Gmelin, B., Philippe, J.-J., Mercker, E., and Preisser, J. S., "HHC Aeroacoustic Rotor Test at the DNW — The Joint German/French/US Project," 20th European Rotorcraft Forum, Amsterdam, The Netherlands, Oct. 1994.

[7]Arnaud, G., and Beaumier, P., "Validation of R85/METAR on the Puma RAE Flight Tests," 18th European Rotorcraft Forum, Avignon, France, Sept. 1992.

[8]Beaumier, P., Prieur, J., Rahier, G., Spiegel, P., Demargne, A., Kube, R., Van der Wall, B. G., Schultz, K. J., Splettstoesser, W., Tung, C., Gallman, J., Yu, Y. H., Brooks, T. F., Burley, C. L., and Boyd, D. D., "Effect of Higher Harmonic Control on Helicopter Rotor Blade-Vortex Interaction Noise: Prediction and Initial Validation," 75th AGARD Fluid Dynamics Panel Meeting and Symposium on Aero-

dynamics and Aeroacoustics of Rotorcraft, Berlin, Germany, Oct. 1994.

[9]Plantin de Hugues, P., ''Study of the Vorticity Trailed at the Blade Tip of a Helicopter Rotor in Hover,'' Ph.D. Dissertation, Univ. of Ain-Marseille II, Dec. 1991.

[10]Rahier, G., ''Modelling of Airfoil-Vortex Interaction and Application to a Helicopter Rotor. Contribution to Blade-Vortex Interaction Noise Prediction,'' Ph.D. Dissertation, Univ. of Paris VI, Oct. 1996.

[11]Kube, R., Splettstoesser, W. R., Wagner, W., Seelhorst, V., Yee, Y. H., Boutier, A., Micheli, F., and Mercker, E., ''Initial Results from the Higher Harmonic Control Aeroacoustic Rotor Test (HART) in the German-Dutch Wind Tunnel,'' 75th AGARD Fluid Dynamics Panel Meeting and Symposium on Aerodynamics and Aeroacoustics of Rotorcraft, Berlin, Germany, Oct. 1994.

[12]Spiegel, P., and Rahier, G., ''Theoretical Study and Prediction of BVI Noise Including Close Interactions,'' American Helicoptor Society Technical Specialists Meeting on Rotorcraft Acoustics and Fluid Dynamics, Philadelphia, PA, Oct. 1991.